Electronic Supplementary Material (ESI) for Journal of Materials Chemistry A.

Coupling isolated Ni single atoms with sub-10 nm Pd nanocrystals embedded in porous carbon frameworks to boost oxygen electrocatalysis for Zn-air batteries

Shangzhi Wang,† Zinan Lin,† Mengmeng Li, Zehan Yu, Minjun Zhang, Mingxing Gong, Yawen Tang,* and Xiaoyu Qiu*

Jiangsu Key Laboratory of New Power Batteries, Jiangsu Collaborative Innovation Center of Biomedical Functional Materials, School of Chemistry and Materials Science, Nanjing Normal University, Nanjing 210023, China

† Equal-contributing authors.

Figures

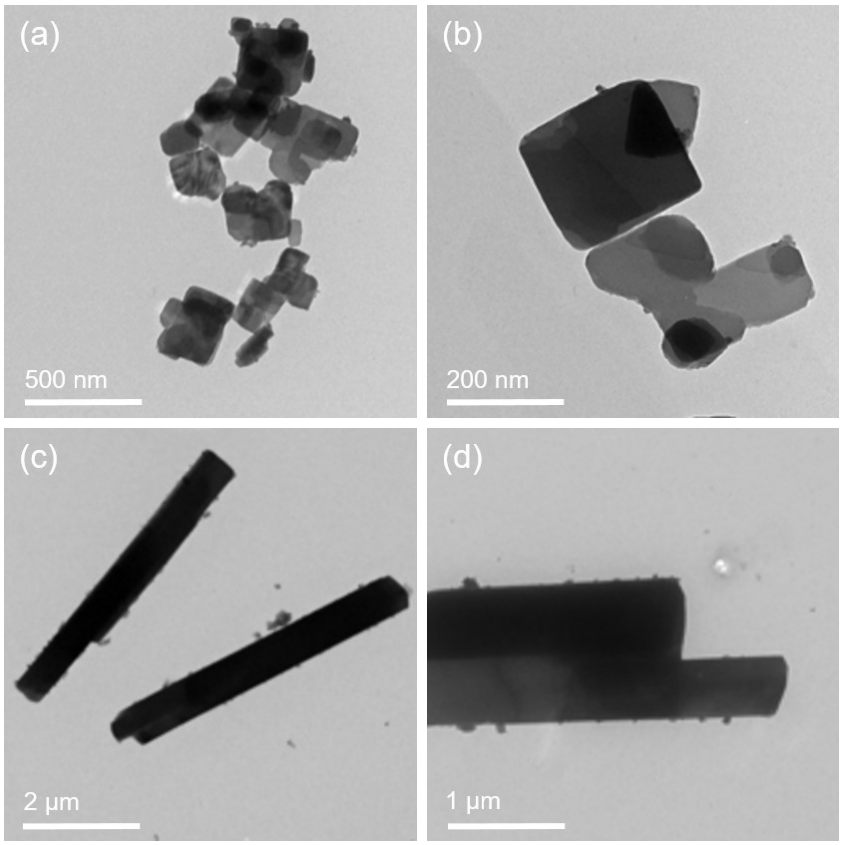

Fig. S1 TEM images of (a)-(b) Pd^{II}-($C_{10}H_7$-NH_2) complex, and (c)-(d) NiPc@Pd^{II}-($C_{10}H_7$-NH_2) complex.

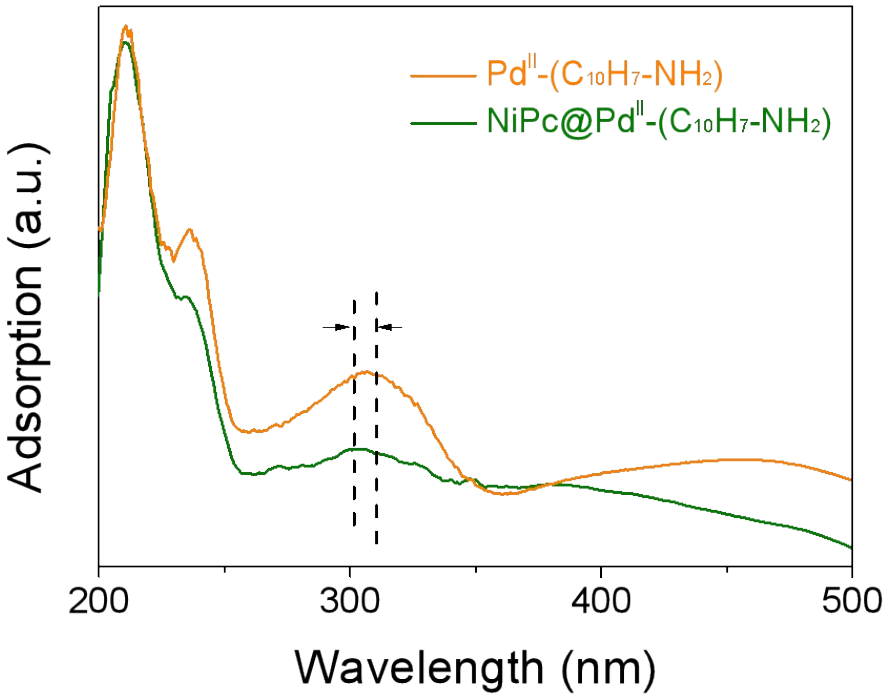

Fig. S2 UV-*vis* spectra of Pd^{II}-(C$_{10}$H$_7$-NH$_2$) solution and NiPc@Pd^{II}-(C$_{10}$H$_7$-NH$_2$) solution.

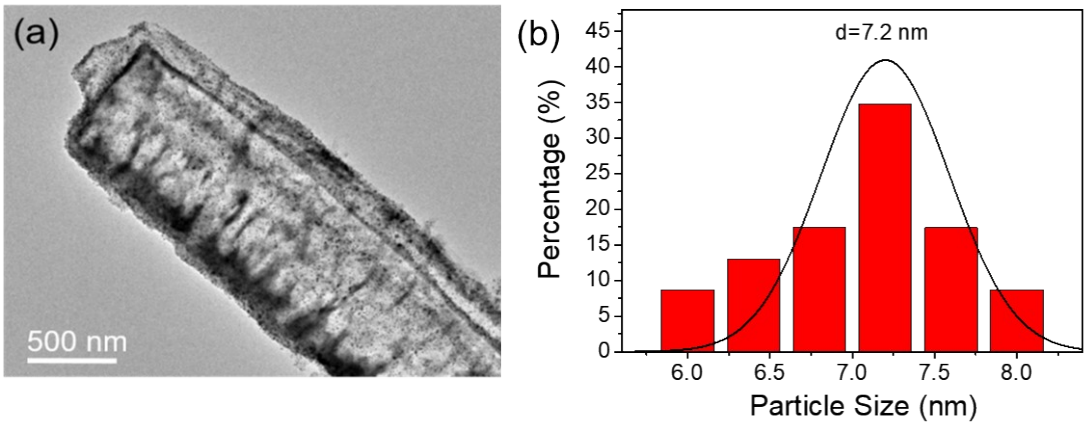

Fig. S3 (a) Representative TEM image of Ni SAs-Pd@NC and (b) corresponding particle size distribution diagram.

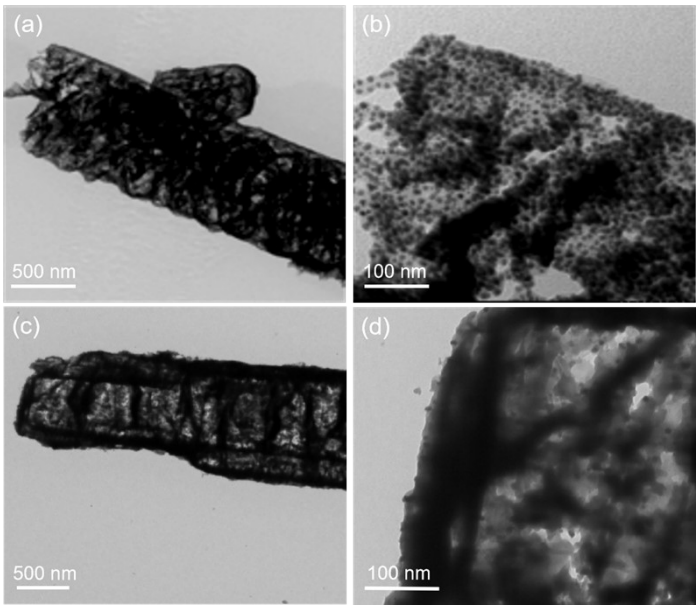

Fig. S4 TEM images of the products prepared using the standard protocol of Ni SAs-Pd@NC except for the feeding ratio of Pd^{II}-($C_{10}H_7$-NH_2) and NiPc. (a)-(b) 4:1, (c)-(d) 1:1.

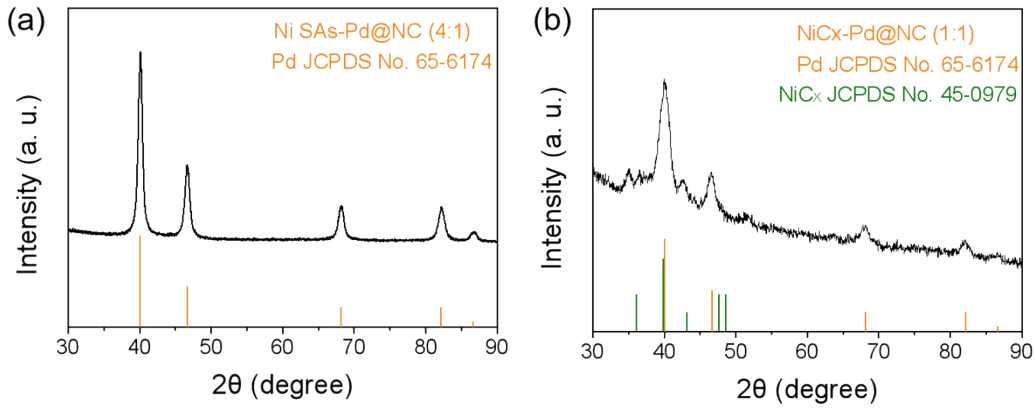

Fig. S5 XRD pattern of the products prepared using the standard protocol of Ni SAs-Pd@NC except for the feeding ratio of Pd^{II}-($C_{10}H_7$-NH_2) and NiPc. (a) 4:1, (b) 1:1.

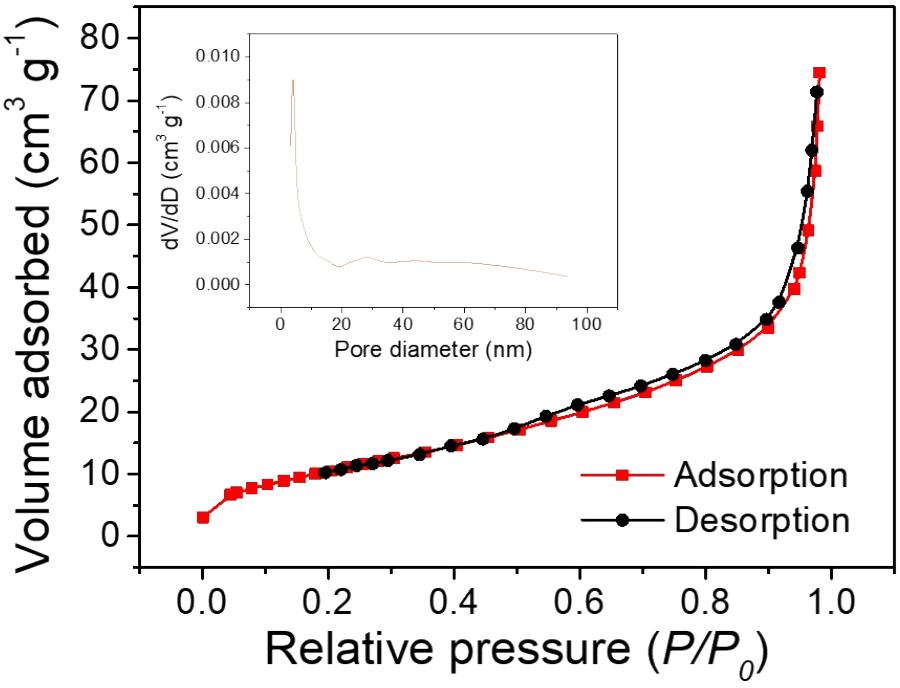

Fig. S6 N_2 adsorption-desorption isotherms of the as-prepared Ni SAs-Pd@NC. Inset shows the pore-size distribution curve.

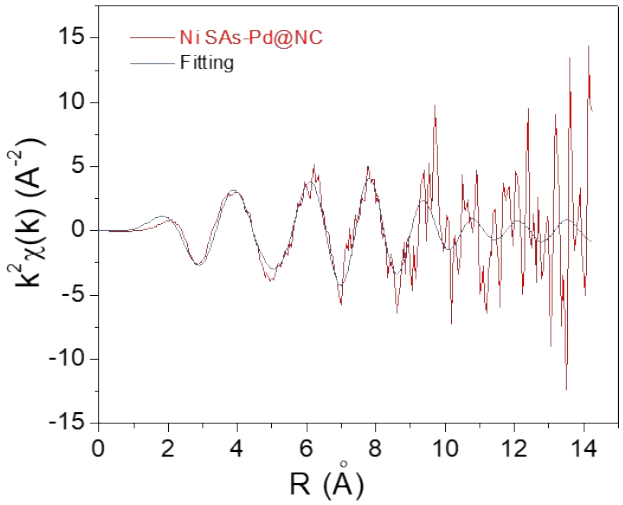

Fig. S7 EXAFS fitting curves of Ni SAs-Pd@NC at K space. The emergence of burrs between 8~14 angstroms could be related to the relative large noise and multiple electron scattering effect of the sample. Due to such obvious noise, the data from 8~14 angstroms may not be the real structure information of the sample. Accordingly, it is possible to show unmatched fitting degree of from 8~14 angstroms.

Table S1. EXAFS fitting parameters at the Ni K-edge for various samples (S_0^2=0.80)

Sample	Shell	N^a	R(Å)^b	$\sigma^2\times10^3$(Å^2)^c	ΔE_0 (eV)^d	R factor
Ni foil	Ni-Ni	12*	2.48±0.01	6.2±0.3	-5.7±0.6	0.002
Ni SAs-Pd@NC	Ni-N	4.1±1.6	2.07±0.04	8.4±6.1	-0.5±2.3	0.013

[a]N: coordination numbers; [b]R: bond distance; [c]σ^2: Debye-Waller factors; [d] ΔE_0: the inner potential correction. R factor: goodness of fit.

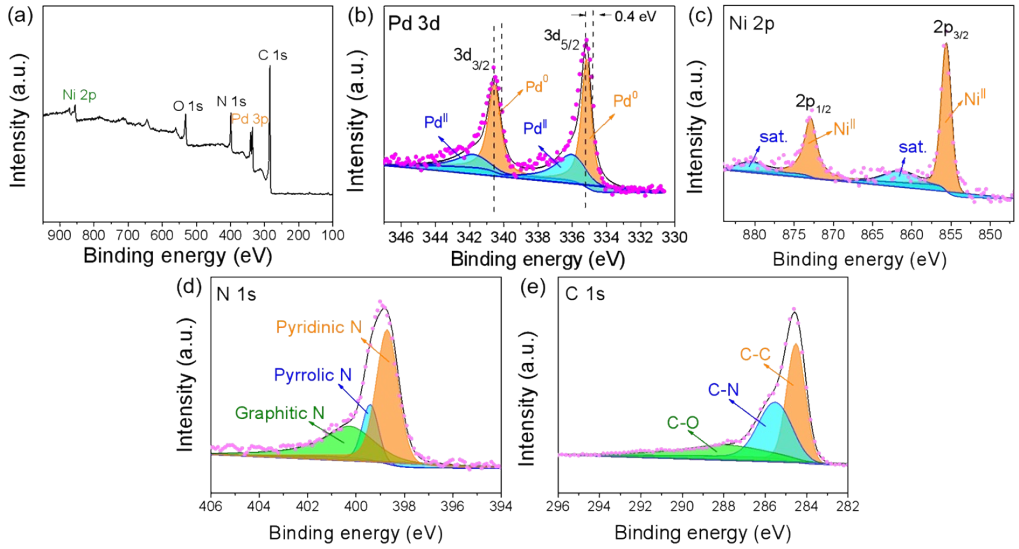

Fig. S8 (a) Full XPS survey of Ni SAs-Pd@NC. High-resolution XPS survey at (b) Pd 3d region, (c) Ni 2p region, (d) N 1s region, (e) C 1s region.

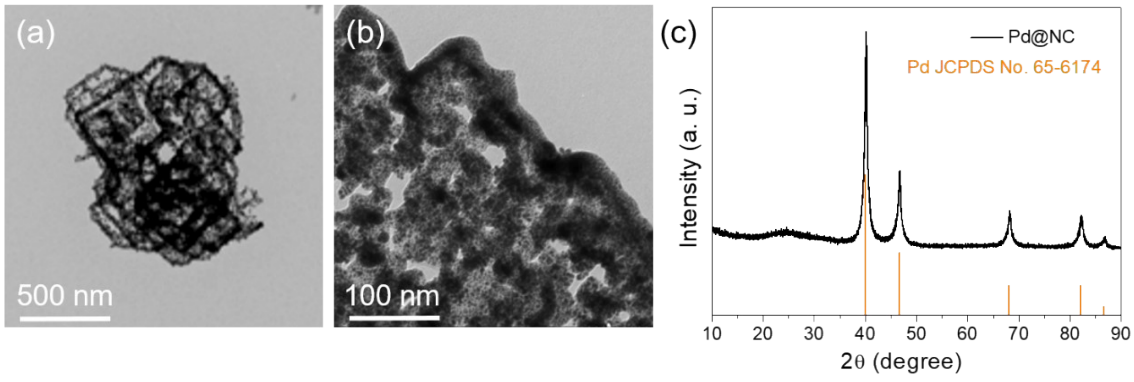

Fig. S9 (a)-(b) TEM images and (c) XRD pattern of Pd@NC.

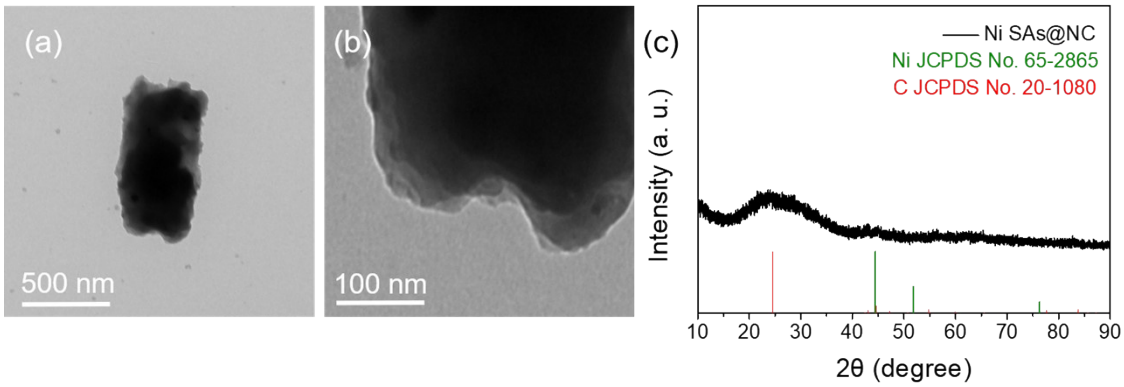

Fig. S10 (a)-(b) TEM images and (c) XRD pattern of Ni SAs@NC.

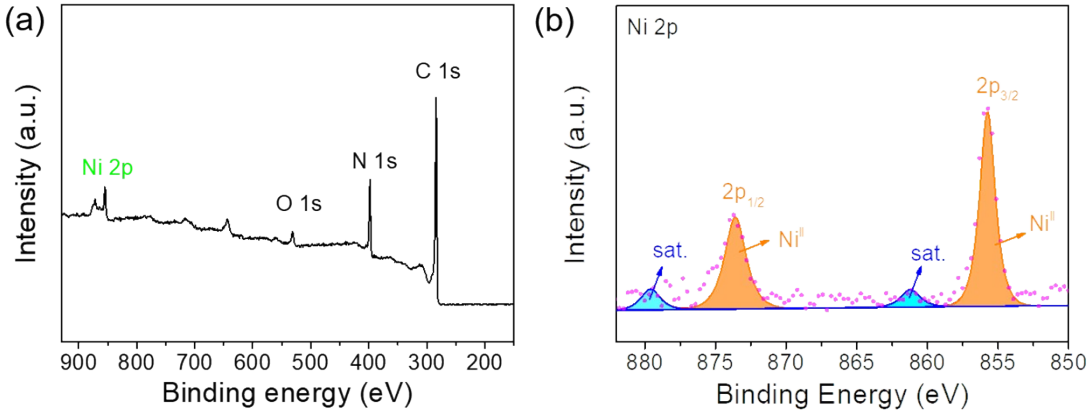

Fig. S11 (a) Full XPS survey of Ni SAs-Pd@NC. (b) High-resolution XPS survey at Ni 2p region.

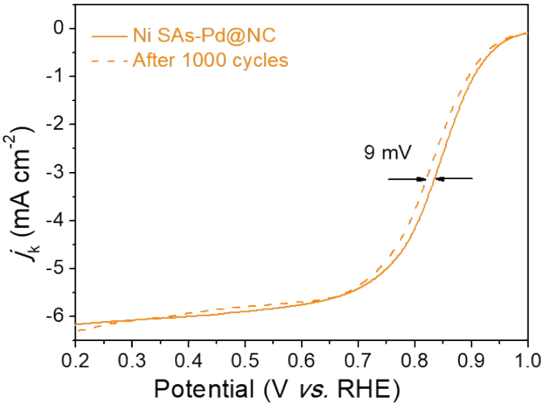

Fig. S12 ORR polarization curves of Ni SAs-Pd@NC before and after ADT.

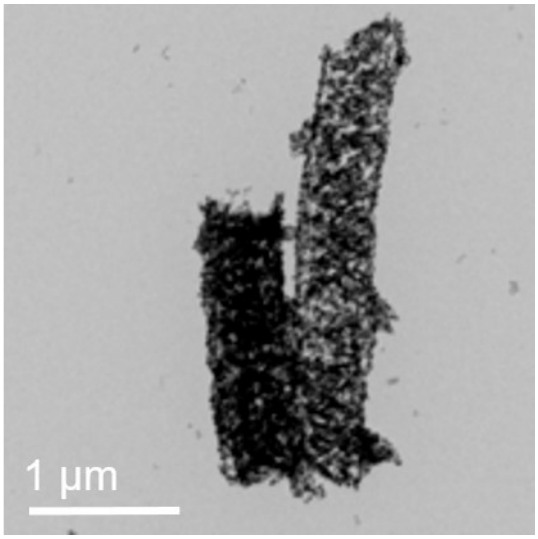

Fig. S13 TEM image of Ni SAs-Pd@NC after the ADT.

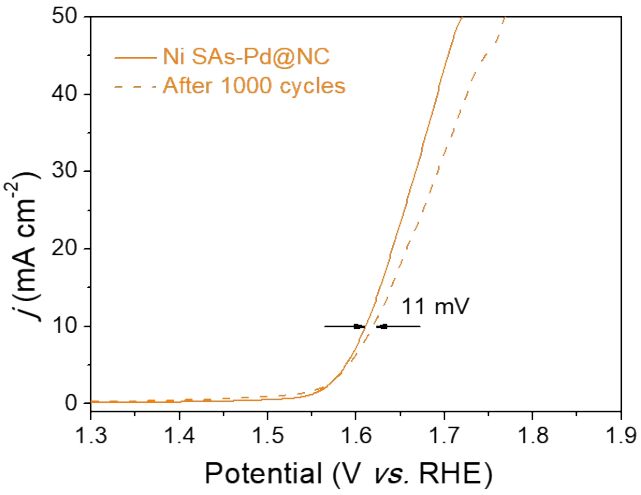

Fig. S14 OER LSV curves of Ni SAs-Pd@NC before and after ADT.

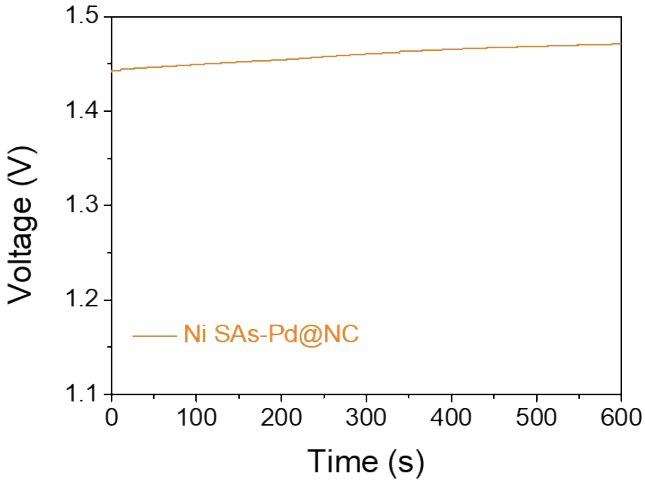

Fig. S15 Open circuit voltage (OCV) curve of Zn-air batteries with Ni SAs-Pd@NC.

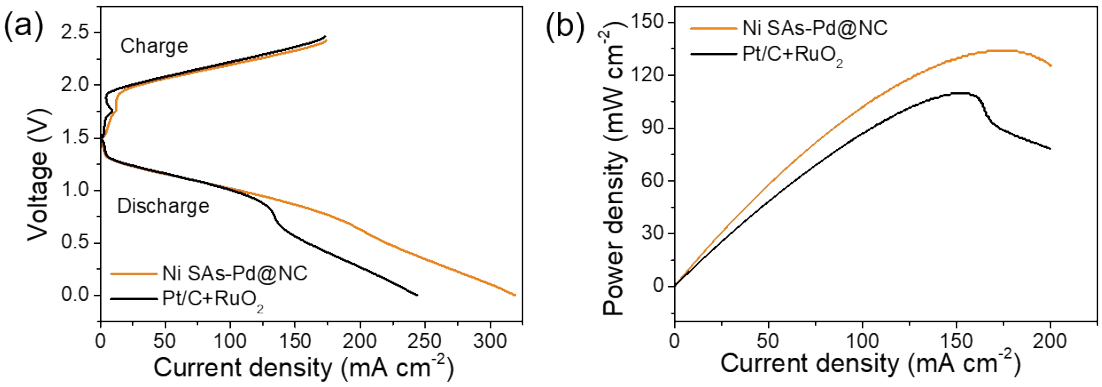

Fig. S16 (a) Charge and discharge polarization curves for rechargeable Zn-air batteries, (b) and corresponding power density curves.

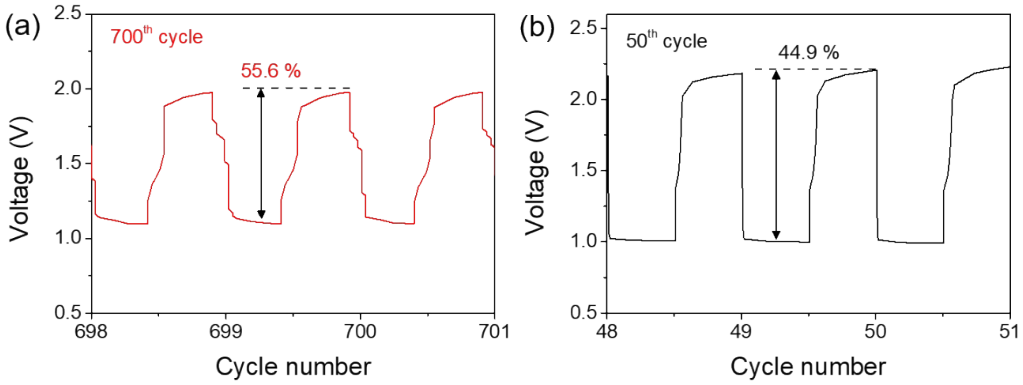

Fig. S17 Discharge and charge voltage profiles of Zn-air batteries with (a) Ni SAs-Pd@NC and (b) Pt/C + RuO_2 at 10 mA cm^{-2}.

Table S2. Comparison of the potential difference between ORR and OER ($\Delta E = E_{j=10} - E_{1/2}$) of Ni SAs-Pd@NC with other electrocatalysts reported previously.

	$E_{1/2}$/V	E_j/V	ΔE/V	Ref.
Ni SAs-Pd@NC	0.84	1.61	0.77	This work
Mn 0.6 (Fe 0.3 Ni 0.7) 0.4 O X Mn	0.81	1.60	0.79	[1]

0.6 (Fe 0.3 Ni 0.7) 0.4 O X Mn 0.6 (Fe 0.3 Ni 0.7) 0.4 O X $Mn0.6(Fe_{0.3}Ni_{0.7})_{0.4}O_x$				
$Co\text{-}600N_2$	0.77	1.55	0.78	[2]
MCCF/NiMn-MOFs	0.70	1.51	0.81	[3]
Co@N-CNTF-2	0.79	1.59	0.80	[4]
CoNP-PTCOF	0.85	1.68	0.83	[5]
W_2N/WC heterostructures	0.81	1.61	0.80	[6]
1/Carbon nanotubes	0.84	1.73	0.89	[7]
$CoO_x@CoN_y$/NCNF550	0.78	1.69	0.91	[8]
ODAC-CoO-15	0.82	1.65	0.86	[9]
4 nm-CoOx/N-RGO	0.83	1.65	0.82	[10]

1. D. M. Morales, M. A. Kazakova, S. Dieckhöfer, A. G. Selyutin, G. V. Golubtsov, W. Schuhmann and J. Masa, *Adv. Funct. Mater.*, 2019, **30**, 1905992.
2. X. He, X. Yi, F. Yin, B. Chen, G. Li and H. Yin, *J. Mater. Chem. A*, 2019, **7**, 6753-6765.
3. W. Cheng, X. Lu, D. Luan and X. Lou, *Angew. Chem., Int. Ed.*, 2020, **59**, 18234-18239.
4. H. Guo, Q. Feng, J. Zhu, J. Xu, Q. Li, S. Liu, K. Xu, C. Zhang and T. Liu, *J. Mater. Chem. A*, 2019, **7**, 3664-3672.
5. J. H. Park, C. H. Lee, J. M. Ju, J. H. Lee, J. Seol, S. U. Lee and J. H. Kim, *Adv. Funct. Mater.*, 2021, **31**, 2101727.
6. J. Diao, Y. Qiu, S. Liu, W. Wang, K. Chen, H. Li, W. Yuan, Y. Qu and X. Guo, *Adv. Mater.*, 2020, **32**, 1905679.
7. L. Xie, X. Zhang, B. Zhao, P. Li, J. Qi, X. Guo, B. Wang, H. Lei, W. Zhang, U.

Apfel and R. Cao, *Angew. Chem., Int. Ed.*, 2021, **60**, 7576-7581.
8. K. Yoon, C. Hwang, S. Kim, J. Jung, J. Chae, J. Kim, K. A. Lee, A. Lim, S. Cho, J. P. Singh, J. M. Kim, K. Shin, B. M. Moon, H. S. Park, H. J. Kim, K. H. Chae, H. C. Ham, I. D. Kim and J. Y. Kim, *ACS Nano*, 2021, **15**, 11218-11230.
9. Y. Tian, X. Liu, L. Xu, D. Yuan, Y. Dou, J. Qiu, H. Li, J. Ma, Y. Wang, D. Su and S. Zhang, *Adv. Funct. Mater.*, 2021, **31**, 2101239.
10. T. Zhou, W. Xu, N. Zhang, Z. Du, C. Zhong, W. Yan, H. Ju, W. Chu, H. Jiang, C. Wu and Y. Xie, *Adv. Mater.*, 2019, **31**, 1807468.